Fiber and Integrated Optics, 21:173–191, 2002

0146-8030/02 $12.00 + .00

Design and Analysis of the Integrated Plasma Wave Micro-Optical Modulator/Switch

SINA KHORASANI
ALIREZA NOJEH
BIZHAN RASHIDIAN

Department of Electrical Engineering
Sharif University of Technology
Tehran, Iran

Feasibility of a new integrated amplitude modulator/switch operating up to the visible spectrum, based on the absorption of light due to the linear interaction of the incident laser and a two-dimensional plasma layer is demonstrated. Plasma layers are generated via the Muller effect at the waveguide's interfaces. A plasma wave is excited in the two-dimensional gas when it is illuminated by electromagnetic radiation. Thus, due to the energy transfer from the electromagnetic wave to the plasma wave, the output light intensity can be controlled. The device is capable of amplitude modulation of guided beams in dielectric waveguides. Analysis based on both full-classical and semiclassical approaches are performed and are compared.

Keywords modulator, switch plasma wave, waveguide optics

Introduction

Rapid growth of electronics technology demands faster and smaller structures. In a recent study, it has been discussed how the propagation of plasma waves in a High Electron Mobility Transistor (HEMT) can be used to implement a new generation of terahertz devices [1]. Presently, a great deal of research is being done on optical structures. Light beams, instead of electric current, will be responsible for carrying information between different parts of these devices and optical circuits. Several approaches for light modulation have been proposed based on electro-optical, magneto-optical, and acousto-optical effects [2]. However, there still exist some fundamental limitations in their sizes and speeds.

Another approach makes use of the interaction of an electric charge and an electromagnetic wave. McQuistan and Schultz [3] proposed an infrared modulator in which free carrier absorption in germanium has been utilized to modulate the radiation. Allen, Tsui, and Vinter [4] investigated the absorption of infrared radiation by electrons in semiconductor inversion layers. Kovacs and Scott [5] demonstrated the optical excitation of surface plasma waves in metal-dielectric interfaces, from both theoretical and experimental points of view. A valuable review of optical plasma resonance has been published by Steinmann [6]. The coupling of light to plasmon oscillations has also been investigated by Lindau and Nilsson [7] and Fontana [8]. Also, a far-infrared light modulator and switch

Received 16 January 2001; accepted 26 October 2001.
Address correspondence to Bizhan Rashidian, Sharif University of Technology, Tehran 11365-9363, Iran. E-mail: rashidia@sina.sharif.edu

has been proposed and developed in the 400 KHz range by Kuijk, Vounckx, Stiens, and Borghs [9–11]. They have used the concept of reflection of light from an inversion layer that acts as a mirror for light frequencies below the layer's plasma frequency. However, it seems that very fast modulation had not been achieved because of the slow dynamics of the inversion layer.

In this article, feasibility of a new voltage-controlled integrated optical modulator/switch, which may be fabricated by existing microtechnology methods, is presented. In this device, the TE or TM polarized laser beam propagates in a planar optical waveguide structure. By means of the Muller effect, which will be discussed in detail, two-dimensional electron gases (2DEGs) are generated at the waveguide's film-cover and film-substrate interfaces. These two-dimensional plasmas can be excited by the light and thus energy transfer between the light beam and the 2DEGs could happen as the result of this interaction. As the amount of light absorption by the electron gases depends on the properties of the 2DEGs such as the charge density in them, it is possible to have a modulator, if one is able to change these properties in a convenient manner. In the Muller effect, a transverse voltage is responsible for the generation and control of the electron gas, and thus the modulation or the switching of the light beam intensity. As will be demonstrated, the device could be operated with low voltages (< 5 V) and power (~ 2.5 mW/μm^2), low switching/modulation time (< 10 ps), and, because of its vertical structure, it can be fabricated in small dimensions. Moreover, the device shows excellent phase behavior, so that amplitude modulation of a guided beam is possible, without violating the dispersion relation of waveguide. As shown, the device is capable of modulating visible light beams. Compared to the approaches for modulating visible beams usually used, including the acousto-optic, magneto-optic, and electro-optic effects [12] at maximum bandwidths well under 10GHz, the proposed device, in addition to its considerably wider bandwidth, has the possibility for being integrated into optical integrated circuits at compact dimensions. Direct amplitude modulation of light is possible also in semiconductor lasers by controlling the electric drive current [13]. However, the structure of our proposed device is much simpler. This permits better and denser integration leading to applications including the integrated optical memory and optical transistor [14], and integrated programmable diffractive element [15] and programmable grating [16]. The preference for operation at visible and shorter wavelengths lies within the fact that the size of waveguide devices vary nearly proportional to the wavelength. Therefore, if the device could operate at a shorter wavelength it could enjoy smaller dimensions which result in better integration, as discussed later in the scaling law of our device.

To analyze the device characteristics, two approaches are followed. In the first approach, being referred to as the full-classical approach, only Maxwell's equations are solved, with the approximation that the charge layer's thickness is negligible. Obviously, this approach is suitable for wavelengths in FIR range, or longer. In the second approach, being referred to as the semi-classical approach, the thickness of the charge layer is calculated by self-consistent solution of Schrödinger's and Poission's equations. This method of self-consistent solution has been widely used in the analysis of HEMT as explained below in more detail. The results are then compared.

Device Structure

The proposed structure is shown in Figure 1. As may be seen in this figure, the device consists of a planar dielectric waveguide in which the light beam propagates. Two metal

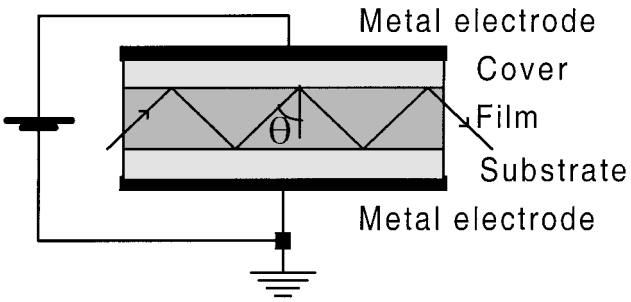

Figure 1. Device structure for the plasma wave optical modulator/switch.

electrodes make it possible to apply a transverse electric field to the waveguide. As is known from the Muller effect, such a voltage will produce a surface electric charge in the interfaces of the dielectrics, if the conductivity to permittivity ratios of these dielectrics are different. This effect has been illustrated in Figures 2(a) and (b). Two neighboring dielectrics standing for the film and cover slabs, as shown in Figure 2(a), may be represented by an equivalent circuit as in Figure 2(b). The voltage is applied across the interface by an external source, which generally results in establishment of an electric current density of free charges normal to the interface. The flow of electric current density leads to accumulation of free interface charges. It can be easily shown that for the film-cover interface, the density of this surface charge is given by the following relationship:

$$\sigma_{fc} = (\rho_s t_s + \rho_f t_f + \rho_c t_c)^{-1}(\rho_f \varepsilon_f - \rho_c \varepsilon_c)V, \tag{1}$$

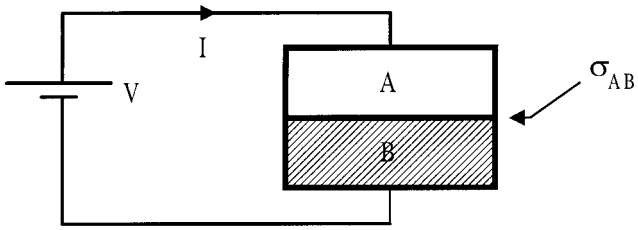

(a)

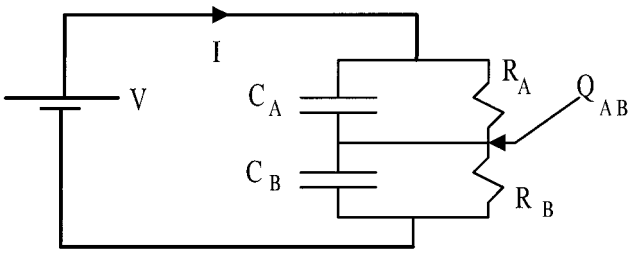

(b)

Figure 2. Illustration of Muller effect: (a) Two dielectrics in contact; (b) Equivalent circuit.

where V is the transverse voltage, t stands for a layer's thickness, and ρ and ε denote resistivity and permittivity, respectively. Also, f, s, and c subscripts refer to film, substrate, and cover layers, respectively. It is seen that the surface charge density is proportional to the applied voltage. If this voltage is changed, the density of the two-dimensional plasma will be changed, causing a change in the reflection coefficient of light, thus modulating the output beam intensity. Proper layer characteristics could be chosen in order to obtain the desired surface charge density with typical voltage values in state-of-the-art CMOS technology (< 5 V).

Method of Analysis

In this section, the method of analysis for the device is described. First, it is shown how a single reflection coefficient from the film-cover interface is calculated, then the amplitude and phase responses are studied. Since we assume a symmetric structure, the same arguments would be applicable for the reflection from the film-substrate interface, too. Then, the amplitude reflection coefficients are compared to the results obtained from a semiclassical approach by self-consistent solution of Poission's and Schrödinger's equations.

Calculation of a Single Reflection Coefficient

In order to calculate the reflection coefficient of light by the structure, one has to solve Maxwell's equations for the system. First, the structure shown in Figure 3 is considered for simplicity, and its reflection coefficient is calculated. The results obtained in this subsection will be used in the complete analysis of the problem in the next subsection. The Silver layer which is shown in the structure accounts for the metal electrode. All mediums are supposed to be simple nonmagnetic and isotropic dielectrics.

Here, only the details of TM polarization are described. For TE polarization a similar approach can be applied. A uniform plane wave is assumed to be incident at the 1-2 boundary at angle θ. The total electric and magnetic fields in region 1 are the sum of the incident and reflected fields. Thus:

$$\begin{aligned} &\mathbf{E}_1 = \mathbf{E}_{inc} + \mathbf{E}_{ref}, && \mathbf{H}_1 = \mathbf{H}_{inc} + \mathbf{H}_{ref} \\ &\mathbf{E}_{inc} = \mathbf{E}_i \exp(-j\mathbf{k}_i \cdot r), && \mathbf{H}_{inc} = \frac{k_1}{\omega\mu_0}\hat{\mathbf{z}} \exp(-j\mathbf{k}_i \cdot \mathbf{r}) \\ &\mathbf{E}_{ref} = \mathbf{E}_r \exp(-j\mathbf{k}_r \cdot \mathbf{r}), && \mathbf{H}_{ref} = \frac{k_1 E_r}{\omega\mu_0}\hat{\mathbf{z}} \exp(-j\mathbf{k}_r \cdot \mathbf{r}), \end{aligned} \tag{2}$$

where $\mathbf{E}$ and $\mathbf{H}$ are the electric and magnetic fields' time-independent harmonic vectors, *inc* and *ref* subscripts refer to the incident and reflected phasors, and E_i and E_r refer to amplitudes of the incident and reflected amplitudes, respectively. Also, $\mathbf{k}$ and $\mathbf{r}$ are the wave and position vectors, and $|\mathbf{k}_i| = |\mathbf{k}_r| = k_1 = \frac{2\pi n_1}{\lambda}$, and $E_i = |\mathbf{E}_i| = 1$. The incident electric field amplitude is assumed to be normalized to unity, ω is the light frequency, and λ and n_1 denote the free space wavelength and the refractive index of region 1, respectively. Also, use has been made of Maxwell's curl equation for writing $\mathbf{H}$ in terms of $\mathbf{E}$. It should be noted that the magnetic field is perpendicular to the plane of the figure for TM polarization and that the electric field lies in that plane.

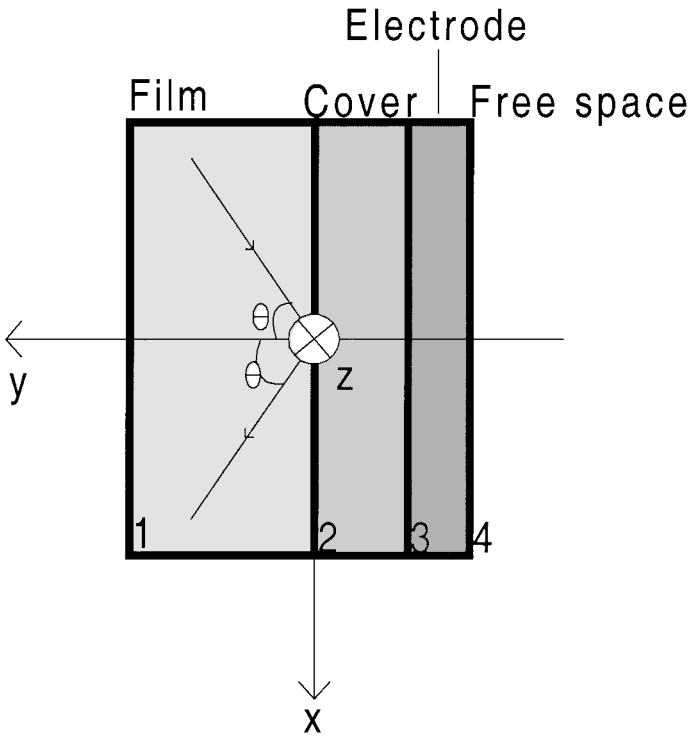

Figure 3. Structure used in the analysis of the optical modulator/switch in Figure 1.

In regions 2, 3, and 4, the electric and magnetic fields are expected to obey the relations

$$\mathbf{E}_l = [S_{lx}(y)\hat{\mathbf{x}} + S_{ly}(y)\hat{\mathbf{y}}]\exp(-jk_{ix}x), \tag{3a}$$

$$\mathbf{H}_l = \left(\frac{\varepsilon_0}{\mu_0}\right)^{1/2}[U_{lz}(y)\hat{\mathbf{z}}]\exp(-jk_{ix}x), \tag{3b}$$

in which the subscript l takes the values 2, 3, or 4. $S(y)$ and $U(y)$ remain as some unknown functions to be determined. The reason for adopting these definitions is that the structure has been assumed to be infinite in the x direction. In addition, it is known that in the case of total internal reflection from 1-2 interface, the energy of the electromagnetic wave propagates only in the x direction and decays in the y direction. Thus, it is reasonable to assume the x behavior of the electromagnetic wave to be like a plane wave. In fact, after the complete solution is found, it will be seen that the electromagnetic wave in regions 2 and 3 is a nonuniform plane wave, i.e., its amplitude depends on the y coordinate. These definitions are similar to those used in [17] for grating diffraction analysis. The above formulae are inserted in Maxwell's curl equations [18], i.e.,

$$\nabla \times \mathbf{E}_l = -j\omega\mu_0\mathbf{H}_l, \tag{4a}$$

$$\nabla \times \mathbf{H}_l = j\omega\varepsilon_0\varepsilon_l\mathbf{E}_l. \tag{4b}$$

After some mathematical manipulation, the following equations result:

$$k_{ix} S_{ly}(y) - j \frac{\partial S_{lx}(y)}{\partial y} = \omega (\mu_0 \varepsilon_0)^{1/2} U_{lz}(y), \tag{5}$$

$$\left(\frac{\varepsilon_0}{\mu_0}\right)^{1/2} \frac{\partial U_{lz}(y)}{\partial y} = j\omega \varepsilon_0 \varepsilon_l S_{lx}(y), \tag{6}$$

$$\left(\frac{\varepsilon_0}{\mu_0}\right)^{1/2} k_{ix} U_{lz}(y) = \omega \varepsilon_0 \varepsilon_l S_{ly}(y). \tag{7}$$

Inserting eqs. (6) and (7) in eq. (5) results in

$$\frac{\partial^2 U_{lz}(y)}{\partial y^2} + [\omega^2 \mu_0 \varepsilon_0 \varepsilon_l - k_{ix}^2] U_{lz}(y) = 0. \tag{8}$$

Based on eq. (8), the magnetic field in regions 2, 3, and 4 is found from

$$U_{lz}(y) = a_l \exp(+j\alpha_l y) + b_l \exp(-j\alpha_l y), \tag{9}$$

with

$$\alpha_l = (\omega^2 \mu_0 \varepsilon_0 \varepsilon_l - k_{ix}^2)^{1/2}. \tag{10}$$

It should be noted that $a_4 = 0$, because region 4 is semi-infinite and only one term suffices for describing the electromagnetic wave in it, either for the propagating mode or for the evanescent situation. In the later case, the first term in the magnetic field in region 4 increases with increasing distance from the 3-4 interface, which is unacceptable. Therefore the first term is omitted.

The solution for the electric field is now simply obtained from eqs. (6) and (7). In the next step, the boundary conditions are imposed. When the transverse voltage is zero, there is no net charge in the interfaces, and the normal and tangential coefficients of the electric field, as well as the tangential coefficient of the magnetic field, are continuous across the boundaries. Applying a transverse DC potential to the system causes an accumulation of net charge at the interface, hence a discontinuity in the DC component of the electric field. As a result of the net charge accumulation, an ac electric current flows parallel to the interface, in response to the incident electromagnetic wave. This ac surface current is given by the following relation:

$$\mathbf{J}_s = (\mu n_s e) E_x \hat{\mathbf{x}}, \tag{11}$$

where μ denotes the mobility of the charges in the electron gas and should not be confused with the permeability. n_s represents the surface carrier density which is equal to σ/e, where e is the fundamental positive electric charge. A discontinuity equal to the amount of this surface current appears in the tangential component of the magnetic field across the interface.

Applying the boundary conditions on the tangential electric and magnetic fields yields a system of six linear algebraic equations which is solved for the unknowns. The reflection coefficient of the structure is then found from

$$ref = E_r E_r^*. \tag{12}$$

A similar analysis has been done for calculating the reflection coefficient for the TE polarized light. Here, the electric field is perpendicular to the plane of the figure and the magnetic field lies in it. The incident magnetic field is assumed to be normalized to unity, and the reflection coefficient is obtained using the following relation:

$$ref = H_r H_r^*. \tag{13}$$

Full-Classical Analysis of the Device

In this subsection, the previous results are used in the complete analysis of the structure, taking also the waveguide's dispersion into account. In the dielectric slab waveguide shown in Figure 1, the following dispersion relation governs the discrete wave propagation modes [19]:

$$2kn_f t_f \cos\theta - 2\Phi_s - 2\Phi_c = 2v\pi, \ v = 0, 1, 2, \ldots, \tag{14}$$

where $k = 2\pi/\lambda$ is the free space wave-vector, and Φ_s and Φ_c stand for the reflection phases from the film-substrate and film-cover boundaries. Thus, one has to know the reflection phases as a function of the incident angle θ in order to be able to solve the dispersion equation. These phases are obtained from the analysis performed in the previous subsection. For each waveguide mode (i.e., for each θ), there exist two reflections in the length Δz of the waveguide given by

$$\Delta z = 2t_f \tan\theta. \tag{15}$$

The decay length Γ of the electromagnetic wave in the waveguide along the z-axis is then defined from the following:

$$\exp\left(-\frac{\Delta z}{\Gamma}\right) = ref_s ref_c. \tag{16}$$

Using eq. (15) in eq. (16) and solving for Γ yields

$$\Gamma = -\frac{2t_f \tan\theta}{\ln(ref_s ref_c)}, \tag{17}$$

which is the required length of the waveguide for having a decay in the wave's amplitude by a factor of e^{-1} (e is the Euler's constant), and may be considered a useful design parameter.

Semiclassical Analysis of the Device

In the semiclassical approach, the effect of thickness of charge layer has been taken into account. It is assumed that the volume density distribution of the charges is governed simultaneously by the Poission's and Schrödinger's equations, so that the application of voltage makes changes in the average density and thickness of the charges. Then an effective complex permittivity constant is assigned to the charge layer, and after then it is treated as a dielectric slab with known thickness and dielectric constants.

Schrödinger's equation may be written in the form

$$\mathbf{H}|n\rangle = \lambda_n |n\rangle, \tag{18}$$

in which $|n\rangle$ is the eigenket of nth state in the system and λ_n is the associated eigenvalue with it. The electronic Hamiltonian $\mathbf{H}$ is defined as [21]

$$\mathbf{H} = -\frac{\eta^2}{2m^*}\frac{d^2}{dz^2} + V(z). \tag{19}$$

The constituting materials and the interface are assumed to be isotropic with regards to the electron effective mass represented by m^*, and the effect of background periodic potential is considered in the value of m^*. The potential energy is related to the electrostatic potential $\Phi(z)$ defined by the relationship

$$V(z) = -q\Phi(z) + \Delta E_c \theta(-z), \tag{20}$$

in which $-q$ stands for the electronic charge, and ΔE_c is the conduction band energy difference across the film and cover interface ($z = 0$). Also θ represents the unit step function. The density of occupied states may be written as [22]

$$N_n = D_n \frac{kT}{q} \ln\left[1 + \exp\left(\frac{E_F - \lambda_n}{kT}\right)\right], \tag{21}$$

where D_n is the density of the nth state [23] given by

$$D_n = \frac{qm^*}{\pi\eta^2}. \tag{22}$$

The energy levels of the unperturbed system with no applied voltage are [24]

$$\lambda_n = \left(\frac{\eta^2}{2m^*}\right)^{1/3}\left[\frac{3}{2}q|\mathbf{E}_s(0)\left(n + \frac{3}{4}\right)\right]^{2/3}. \tag{23}$$

Here, $\mathbf{E}_s(0)$ stands for the discontinuity of normal electric field at the interface due to the 2D electron gas and may be expressed as

$$|\mathbf{E}_s(0)| = q\frac{n_s}{\varepsilon_{eff}}, \tag{24}$$

in which the effective dielectric permittivity at the contact interface is defined as $\varepsilon_{\text{eff}} = \varepsilon_0 (\varepsilon_c + \varepsilon_f)/2$ [18]. Also, the electrostatic potential obeys the Poission's equation:

$$\nabla^2\Phi(z) = -\frac{\rho(z)}{\varepsilon}, \tag{25}$$

in which $\rho(z)$ is the effective charge density:

$$\rho(z) = -q\sum_n N_n |\langle z|n\rangle|^2. \tag{26}$$

Here, N_n is the density of occupied states, and $\langle z|n\rangle$ is the electron wave function at nth state.

The numerical method solves the system of second-order differential equations:

$$\frac{d^2}{dz^2}\begin{bmatrix}\Phi(z)\\ \langle z|0\rangle_0\\ \langle z|1\rangle_0\\ \cdot\\ \cdot\\ \langle z|n\rangle_0\end{bmatrix} = \begin{bmatrix} -\dfrac{q}{\varepsilon_{eff}}\displaystyle\sum_n N_n|\langle z|n\rangle_0|^2 \\ \dfrac{2m^*}{\eta^2}[V(z)-\lambda_{00}]\langle z|0\rangle_0 \\ \dfrac{2m^*}{\eta^2}[V(z)-\lambda_{10}]\langle z|1\rangle_0 \\ \cdot \\ \cdot \\ \dfrac{2m^*}{\eta^2}[V(z)-\lambda_{n0}]\langle z|n\rangle_0 \end{bmatrix}, \tag{27}$$

subject to the boundary conditions

$$\begin{aligned} \langle z|n\rangle|_{z=-t_f} &= 0, \\ \langle z|n\rangle|_{z=t_c} &= 0, \\ \Phi(z)|_{z=-t_c} &= V, \\ \Phi(z)|_{z=t_f} &= 0. \end{aligned} \tag{28}$$

In eq. (27) the zero subscript denotes the unperturbed states without voltage across the interface.

Now, the following finite difference approximation [25, 26]

$$\frac{d^2}{dz^2}A(z) \approx \frac{A(z_{n+1}) + A(z_{n-1}) - 2A(z_n)}{\Delta z^2} \tag{29}$$

is applied to solve the system in eq. (27). Of course, the unperturbed wave functions appear in the first equation as well, thus complicating the numerical method. By repeated solution of eq. (27), however, it is possible to achieve convergence with reasonable iterations.

Then, the perturbed eigenvalues are found from the relations

$$\lambda_k = \lambda_{k0} + \Delta\lambda_k, \tag{30}$$

$$\Delta\lambda_k \approx \langle k|\Delta\mathbf{H}|k\rangle. \tag{31}$$

This is the standard perturbation technique as applied in quantum mechanics [27].

Finally, the average density of electron gas $\langle\rho\rangle$ and effective thickness $\langle t\rangle$ are derived from

$$\begin{aligned} \langle\rho\rangle &= \sum_n N_n\langle|\langle z|n\rangle|^2\rangle, \\ \langle t\rangle &= -\frac{\sigma_{fc}}{q\langle\rho\rangle}. \end{aligned} \tag{32}$$

This information are used in defining the frequency dependent complex permittivity of the electron gas layer. In the collisionless limit it is given as [28]

$$\varepsilon = \varepsilon_{eff}\left(1 - \frac{\omega_p^2}{\omega^2}\right) + j\left(\frac{q\mu}{\omega}\langle\rho\rangle\right). \tag{33}$$

Here, $\omega_p^2 = q^2\langle\rho\rangle/m^*\varepsilon_{eff}$ is the so-called plasma frequency, μ is the interface mobility, and j is the unit imaginary number. The real part of the above relation represents the total electrical behavior of the electron gas, while the imaginary term represents its electrical conductivity.

The rest of this approach is similar to the previous subsection, but with a finite thickness electron gas layer inserted between the film and cover layers instead of a simple current sheet.

Results and Discussions

A typical structure has been analyzed based on the above formulation. The dielectric regions can be made up of transparent conductors such as ITO (Indium Tin Oxide) or ZnO (Zinc Oxide). One can control the degree of transparency and conductivity to a large extent in the process of depositing these materials. In our example, an index of refraction equal to 1.8 is assumed for the film region (region 1 in Figure 3). It should be pointed out that interface mobility is greater than the bulk mobility, because interface states are present at the interface and carriers in these states are not bounded to the lattice to the degree that the bulk states are. This is why the use of dielectrics in the structure does not cause any difficulty. Meanwhile, the interface mobility may be increased by either depositing a thin layer (a few monolayers) of a high electron mobility material or reducing the operation temperature. For the second region (the cover), a refractive index equal to 1.4 has been assumed. For the Ag electrode, the value of the relative permittivity has been taken as $-12 + j\,0.4$ for the wavelength used in the analysis [20]. Also, $t_2 = 100$ nm and $t_3 = 20$ nm with resistivities $\rho_s = \rho_c = 10^{-2}\ \Omega m$ and $\rho_f = 10^{-1}\ \Omega m$ have been chosen for the calculations.

The calculated classical reflection coefficient for a visible incident laser beam (4950 A°) as a function of incident angle is plotted in Figure 4 for both TM and TE polarizations. In the TM case, it is seen that there exists a deep minimum in the curve that is known to be due to the excitation of a surface plasma wave (SPW) at the electrode-cover interface. This plasma wave absorbs energy from the incident beam and reduces the reflected light intensity. Such a minimum is not observed in the TE mode, because the TE polarized light does not have a coefficient of the electric field perpendicular to the interface, and thus it can not generate a surface electric charge. Next, it is assumed that a transverse voltage is applied to the system. A net charge density is generated at the film-cover interface as the result of the Muller effect. This net charge produces a net surface electric current that appears in the continuity relation for the magnetic field at the interface under consideration. The corresponding equations are again solved and the resulting reflectance is plotted as a function of the angle of incidence in Figure 4 for different values of the applied external voltage.

As may be observed from the figure, the reflectance curve is shifted to lower values after the voltage is applied to the system, for both TM and TE modes. This general reduction of the reflected power throughout the curve is attributed to the excitation of a surface plasma wave at the film-cover interface. It is also possible to plot the classical reflectivity versus the applied voltage, at a fixed angle (Figure 5). This curve shows the light intensity modulation caused by the applied voltage for different values of interface mobility at the fixed angle of incidence of 50°. In addition, the excellent switching capability of the device is seen from the figure, as the application of 5V to the system causes the reflection coefficient to fall from 0.9 to 0.1, interface mobility of $4m^2/VSec$ and TM polarization. For the TE case, a 5V transverse voltage causes a reduction in reflectivity from 1 to 0.1.

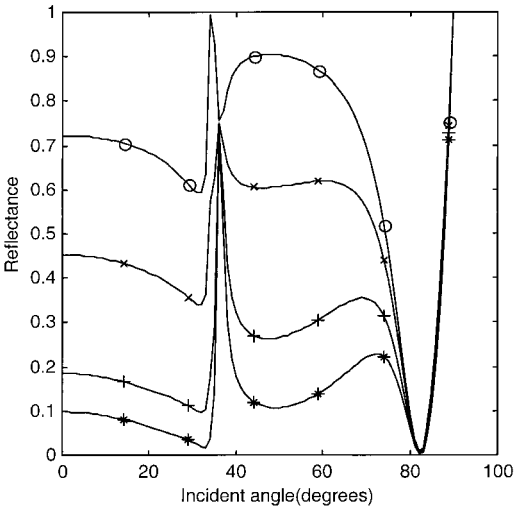

(a)

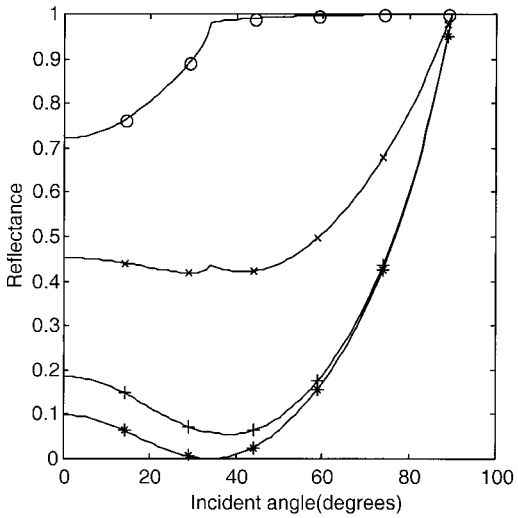

(b)

Figure 4. Dependence of reflectivity on incident angle: (o) No applied voltage, (x) V = 1V, (+)V = 3V, (*)V = 5V (Interface mobility = $5m^2$/VSec). (a) TM polarization; (b) TE polarization.

Next, the waveguide shown in Figure 1 is considered. The difference between single classical reflection phases for 0V and 5V applied transverse voltages is plotted in Figure 6 for TM and TE modes, as a function of the incident angle. An interface mobility equal to $1m^2$/VSec has been assumed. As it is seen from the figure, the application of a small (< 5V) transverse voltage causes no significant change in the reflection phase and thus leaves the wave propagation modes approximately unchanged in the waveguide. This feature is extremely important in the modulator application of the device. If this characteristic did not exist, the change in the transverse voltage would have brought

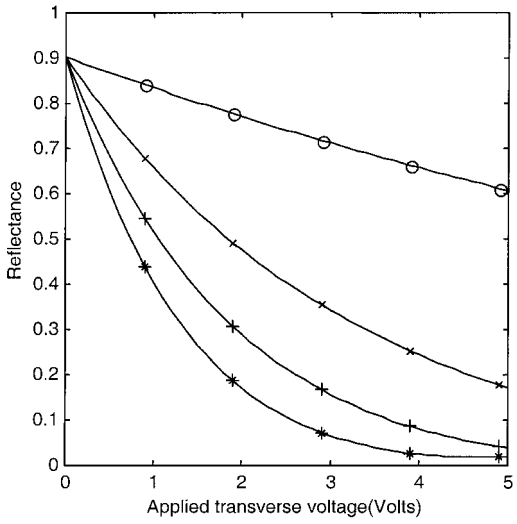

(a)

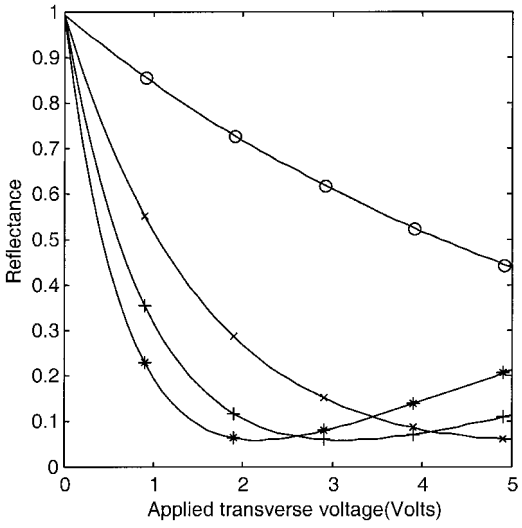

(b)

Figure 5. Dependence of reflectivity on the transverse voltage: (o), Interface mobility = $1m^2$/VSec; (x), Interface mobility = $4m^2$/VSsec; (+), Interface mobility = $7m^2$/VSec; (*), Interface mobility = $10m^2$/Vsec. (a) TM polarization; (b) TE polarization.

a propagating mode to a cut-off mode and it would have been impossible to have a modulated output in a fixed propagation angle θ (i.e., in a fixed propagation mode). It should be pointed out that increasing the interface mobility severely affects this feature. For interface mobilities about $5m^2$/VSec, the reflection phase greatly changes by changing the applied voltage, and as a consequence wave propagation modes change and the device can only be used as a switch and not a modulator.

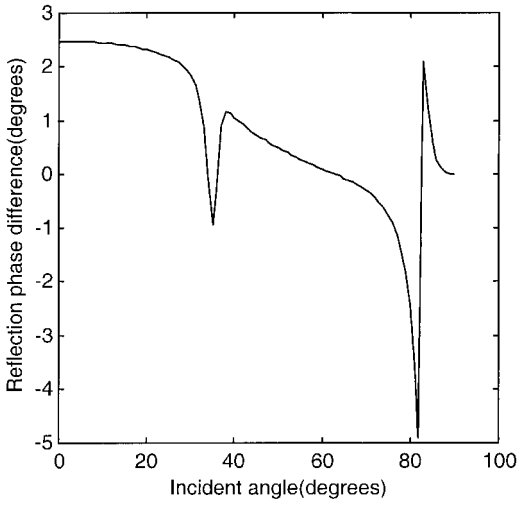

(a)

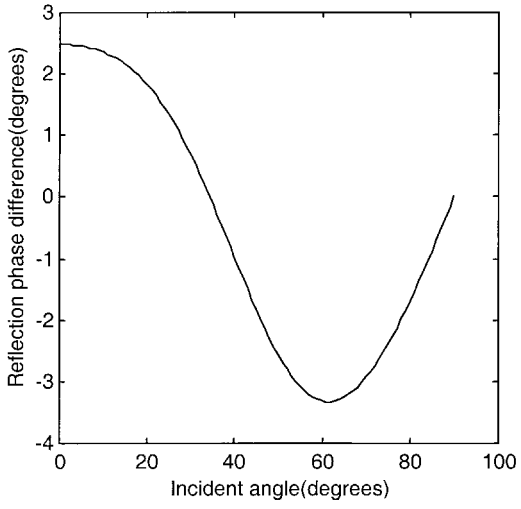

(b)

Figure 6. Dependence of reflection phase difference between 0V and 5 applied voltage cases on the incident angle (Interface mobility = $1m^2/VSec$). (a) TM polarization; (b) TE polarization.

In Figure 7, the dependence of the decay length defined by eq. (17) on the propagation angle (mode) is shown for several transverse voltages. The interface mobility has been assumed to be equal to $1m^2/VSec$ which is an appropriate value for the reflection phase to be independent of the transverse voltage. Although the reflectivity variation as a function of the voltage is weaker in smaller values of mobility, one must take into account the fact that the light undergoes several reflections in the waveguide and the overall modulation of the output intensity will be considerable, for it is the product of all reflection coefficients. This is why reasonable decay lengths are obtained (Figure 7). It should also be considered

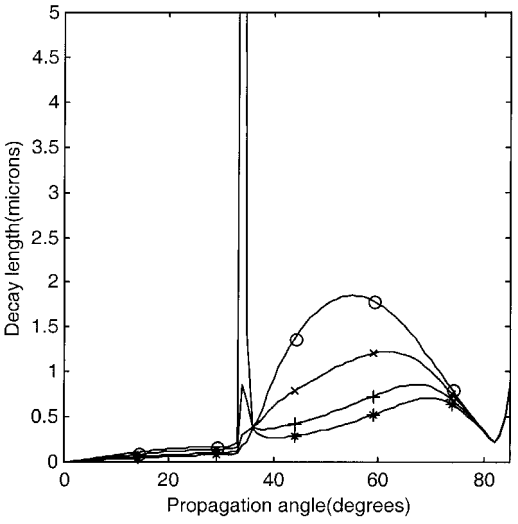

(a)

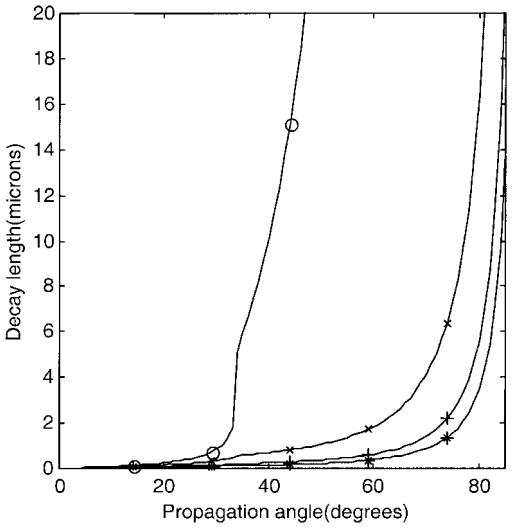

(b)

Figure 7. Dependence of the decay length along the waveguide axis on the propagation angle: (o), No applied voltage; (x), V = 1V, (+)V = 3V; (*), V = 5V (Interface mobility = $5m^2/VSec$). (a) TM polarization; (b) TE polarization.

that only a set of discrete angles is allowed for propagation and the curve does not have any meaning for angles out of that set.

In Figure 8 the results of semiclassical analysis for the effective thickness and density of the gas layer as given by eq. (32) are drawn, for a potential step of 0.1eV in the conduction bands across the interface. It is observed that for voltages below 2V, the variations are nearly linear. Higher voltages lead to large effective thickness above 0.1μm,

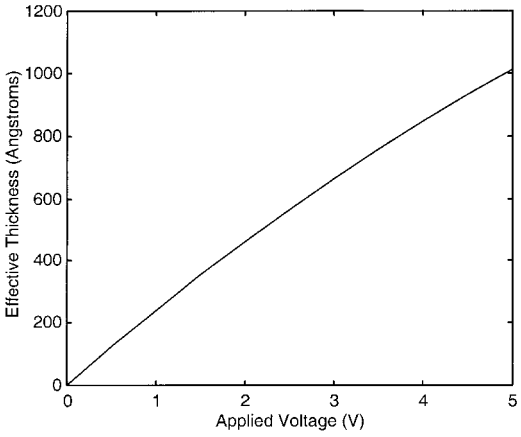

(a)

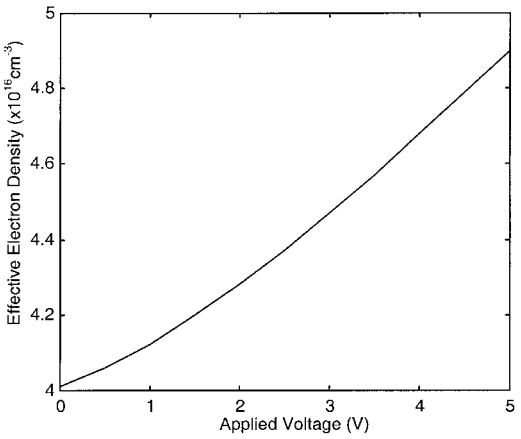

(b)

Figure 8. Dependence of charge layer's properties vs. applied voltage: (a) Effective thickness; (b) Effective density.

far from the practice. This is due to the fact that at higher voltages, the accuracy of the first-order perturbation fails down due to a larger potential gradient. Furthermore, considering the shape of wave functions at the film-cover interface, which has a large peak and long tails, averaging will result in this relatively large effective thickness. To be able to make a comparison between the classical and semiclassical calculations, the dependence of reflectivity on the angle of incidence versus the applied voltage same as in Figure 4, are plotted for TM and TE excitations in Figure 9. A reasonable agreement between the corresponding curves can be noticed for the applied voltages of 0.1 and 1V. Of course, as discussed earlier, inaccuracy of semiclassical analysis at higher voltages has led to many distorted behaviors at 3V and 5V. Of course, one expects to get improved results both with applying a higher-order perturbation technique or a more exact non-linear numerical scheme, as well as taking the effect of collisions into account. For larger

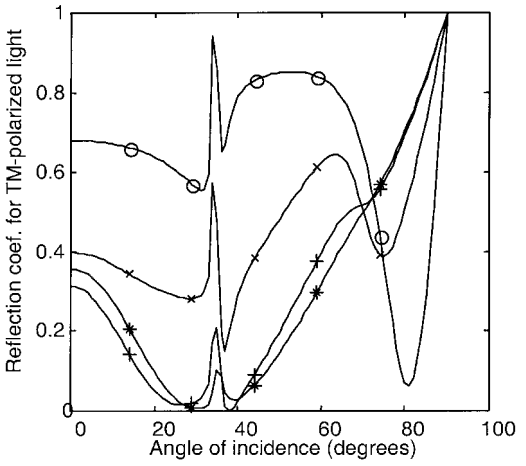

(a)

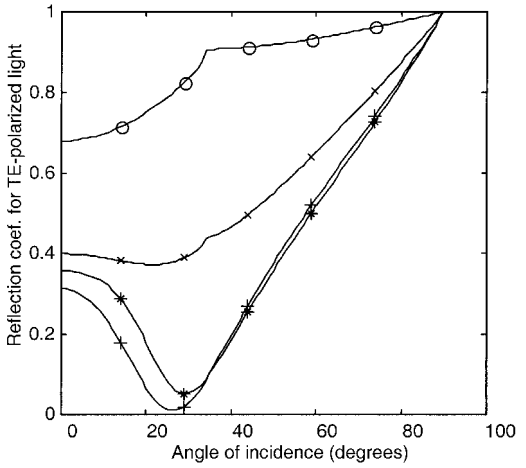

(b)

Figure 9. Dependence of reflectivity on incident angle—Semiclassical analysis: (o), V = 0.1V; (x), V = 1V; (+), V = 3V; (*), V = 5V (Interface mobility = 5 m^2/V.sec): (a) TM polarization; (b) TE polarization.

wavelengths (above 5 mm), the classical approach is expected to give more accurate results. This is obviously due to the small thickness of the charge layer compared with the wavelength.

A critical point to be considered here is the device's speed. The speed limiting mechanism in this device is the time constant that accounts for charge accumulation in the interfaces and is equal to the sum of three time constants, each of which describes one of the three regions of the waveguide:

$$\tau = R_s C_s + R_f C_f + R_c C_c = \rho_s \varepsilon_s + \rho_f \varepsilon_f + \rho_c \varepsilon_c, \tag{34}$$

where R and C denote resistance and capacitance, respectively. In our example, τ is calculated to be 2.64ps, and it is hence concluded that up to more than 100GHz switching is possible. It is seen that τ is independent of the structure's dimensions and depends only on layers' resistivities and permittivities. Eq. (1) shows that changing all the resistivities by the same factor does not affect the surface charge density, and so leaves the reflectivity unchanged for a given applied voltage. On the other hand, a decrease in the resistivities causes a decrease in τ, thus speeding up the device. But it also increases the transverse DC current that is a consequence of the Muller effect. Hence, the overall power dissipation is increased. Also, it is seen from eq. (11) that an increase in the carrier mobility increases the surface current that absorbs energy from the incident beam and thus decreases the reflectivity. One interesting point to be considered here is that the dependence of the reflectivity on the applied voltage for a fixed angle is approximately linear for smaller values of interface mobility (interface mobility = $1\text{m}^2/\text{VSec}$). This feature is seen in Figure 4. So, the amplitude modulator is linear to a large extent. Increasing the value of interface mobility increases the energy absorption by the surface current, but as is seen from Figure 4, it decreases the linearity of the modulator. The dissipation power at a voltage of 5V is estimated to be about 2.5 $\text{mW}/\mu\text{m}^2$.

It is also interesting to discuss the wavelength dependence of the device. If the wavelength of the laser beam is changed by an arbitrary factor, not only the structure dimensions but also the applied voltage has to be increased by the same factor in order to have the same result. Because increasing layer thicknesses causes a decrease in the generated interface charge as is seen from eq. (1), thus the transverse voltage should be increased by the same factor in order for the interface charge to remain constant. Generally speaking, the performance of the device becomes better for larger wavelengths. The higher the wavelength, the better the classical behavior of the device, and thus the better the performance.

Conclusions

A waveguide structure for modulating the intensity of a visible laser beam by means of a transverse applied electric field has been proposed. The two-dimensional plasmas which are produced at the waveguide's film-cover and film-substrate interfaces as the result of the Muller effect are responsible for the absorption of power from the incident beam and the modulation of the output intensity. The analysis was done through classical and semi-classical approaches and the results were in agreement, especially at low voltages. The proposed device may be fabricated by existing microtechnologies and has much potential for use in optoelectronics integrated circuits. It has numerous potential applications in the technology of integrated optical computing.

References

1. Dyakonov, M. I., and M. S. Shur. 1996. Plasma wave electronics: Novel terahertz devices using two dimensional electron fluid. *IEEE Transactions on Electron Devices*, 43:1640–1645.
2. Yariv, A., and P. Yeh. 1984. *Optical Waves in Crystals*. New York: John Wiley and Sons.
3. McQuistan, R. B., and J. W. Schultz. 1964. Modulation of infrared by free carrier absorption. *Journal of Applied Physics*, 35:1243–1248.
4. Allen, Jr., S. J., D. C. Tsui, and B. Vinter. 1976. On the absorption of infrared radiation by electrons in semiconductor inversion layers. *Solid State Communications*, 20:425–428.
5. Kovacs, G. J., and G. D. Scott. 1977. Optical excitation of surface plasma waves in layered media. *Physical Review B*, 16:1297–1311.

6. Steinmann, W. 1968. Optical plasma resonances in solids. *Physica Status Solidi*, 28:437–462.
7. Lindau, I., and P. O. Nilsson. 1970. Experimental evidence for excitation of longitudinal plasmons by photons. *Physics Letters A*, 31:352–353.
8. Fontana, E. 1998. A theoretical analysis of the coupling of light to surface-plasmon oscillations at the edge of a slab waveguide. *IEEE Transactions on Microwave Theory and Techniques*, 46:234–241.
9. Kuijk, M., and R. Vounckx. 1989. Use of two-dimensional electron gas in optical information processing: Proposal for integrated mirror optical switch. *Electronics Letters*, 25:231–233.
10. Stiens, J., M. Kuijk, R. Vounckx, and G. Borghs. 1991. New modulator for far-infrared light: Integrated mirror optical switch. *Applied Physics Letters*, 59:3210–3212.
11. Kuijk, M., and R. Vounckx. 1989. Optical plasma resonance in semiconductors: Novel concepts for modulating far-infrared light. *Journal of Applied Physics*, 66:1544–1548.
12. Yariv, A., and P. Yeh. 1984. *Optical Waves in Crystals*. New York: John Wiley & Sons.
13. Verdeyen, J. 1995. *Laser Electronics*, 2nd ed. Englewood Cliffs, NJ: Prentice Hall.
14. Khorasani, S., A. Nojeh, and B. Rashidian. 2001. A new integrated optical memory based on the plasma wave modulator/switch. *Proc. SPIE*, 4277:311–314.
15. Rashidian, B., and S. Khorasani. 2001. A new integrated programmable optical diffractive element. *Proc. SPIE*, 4277:428–434.
16. Rashidian, B., and S. Khorasani. 2001. Design and analysis of the plasma wave based programmable grating. To be published in *Proc. SPIE*, 4598.
17. Glytsis, E. N., and T. K. Gaylord. 1990. Three-dimensional (vector) rigorous coupled-wave analysis of anistrotropic grating diffraction. *Journal of the Optical Society of America A*, 7:1399–1420.
18. Cheng, D. K. 1989. *Field and Wave Electromagnetics*, 2nd ed., New York: Addision-Wesley.
19. Kogelnik, H. G. 1975. Theory of dielectric waveguides. in *Integrated Optics*. Edited by T. Tamir and E. Gamir. Berlin: Springer-Verlag.
20. Johnson, P. B., and R. W. Christy. 1972. Optical constants of the noble metals. *Physical Review B*, 6:4370–4379.
21. Stern, F., and S. D. Sarna. 1984. Electron energy levels in GaAs-$Ga_{1-x}Al_xAs$ heterojunctions. *Physical Review B*, 30:840–848.
22. Ando, T. 1976. Density functional calculations of sub-band structure in accumulation and inversion layers. *Physical Review B*, 13:3468–3477.
23. Ali, F., and A. Guppta, eds., 1991. *HEMTs and HBTs: Devices, Fabrication and Circuits*. Boston: Artech House.
24. Stern, F. 1974. Quantum properties of surface space charge layers. *CRC Critical Reviews in Solid-State Science*: 499–512.
25. Sadiku, M. N. O. 1992. *Numerical Techniques in Electromagnetics*. Boca Raton: CRC Press.
26. Gerlad, C. F., and P. O. Wheatley. 1989. *Applied Numerical Analysis*, 4th ed., Reading: Addision Wesley.
27. Sakurai, J. J. 1985. *Modern Quantum Mechanics*. Redwood City: Addision Wesley.
28. Kong, J. A. 1975. *Theory of Electromagnetic Waves*. New York: John Wiley & Sons.

Biographies

Sina Khorasani received his BSc (with the highest honor) from Abadan Institute of Technology, and his MSc (1996) and PhD (2001) from Sharif University of Technology, all in Electrical Engineering. He is now assistant professor of Electrical Engineering Department at Sharif University of Technology.

Alireza Nojeh received his BSc (1997) and MSc (1999) in Electrical Engineering from Sharif University of Technology. He is now PhD Candidate at Department of Electrical Engineering of Stanford University.

Bizhan Rashidian received his BSc and MSc (with the highest honor) from Tehran University, and his PhD from Georgia Institute of Technology, all in Electrical Engineering in 1987, 1989, and 1993, respectively. He has been with Department of Electrical Engineering of Sharif University of Technology since 1994, where he is now associate professor, and the funding director of microtechnology lab, and photonics lab. His active research areas include: optics, micromachining, microelectronics, and ultrasonics.